

# 1 **Comparisons of corrosion behaviour for X65 and low Cr steels in high** 2 **pressure CO<sub>2</sub>-saturated brine**

3 Yong Hua\*, Sikiru Mohammed, Richard Barker and Anne Neville

4 Institute of Functional Surfaces, School of Mechanical Engineering, University of Leeds,  
5 Leeds, LS2 9JT, United Kingdom.

6 \*Corresponding author: Yong Hua, Ph.D., Tel: +44 (0) 7923359918, fax: +44 (0) 1132424611.

7 *Email address:* [menyh@leeds.ac.uk](mailto:menyh@leeds.ac.uk) (Y. Hua)

8

9 Appropriate material selection for injection pipelines and tubing for carbon dioxide geologic  
10 storage is fundamental to ensure asset integrity and reduce cost. This paper evaluates the  
11 corrosion behaviour of X65, 1Cr, 3Cr and 5Cr, which have the potential to be utilised as injection  
12 pipeline/tubing materials. The influence of steel Cr content on the general and localised  
13 corrosion behaviour is investigated at time periods from 6 to 192 hours at 60°C and 100 bar.  
14 The evolution, morphology and chemistry of corrosion products on the surface of each material  
15 were evaluated using a combination of Scanning Electron Microscopy, Energy Dispersive X-Ray  
16 Spectroscopy and X-Ray Diffraction and related to their overall corrosion protection. Results  
17 indicate that prior to the formation of protective films on the steel surfaces, the resistance of  
18 the materials to corrosion increase with increasing Cr content (Corrosion resistance:  
19 X65<1Cr<3Cr<5Cr). However, as corrosion products evolve, the protection afforded to the  
20 different steels varies significantly and decreases with increasing Cr content. X65 becomes the  
21 material with the lowest general corrosion rate by the end of the 192 h experiments and 5Cr  
22 exhibits the highest corrosion rate (ranking of corrosion resistance: X65>1Cr>3Cr>5Cr). In terms  
23 of the corrosion products on X65, both inner amorphous and outer crystalline corrosion layers  
24 consist of FeCO<sub>3</sub>. For the Cr-containing steels, the outer layer also comprises FeCO<sub>3</sub>, but the  
25 inner layer is enriched with Cr, and is predominantly amorphous Cr(OH)<sub>3</sub>. The extent of localised  
26 corrosion (determined using surface profilometry) is noticeably less for X65 compared to the Cr-  
27 containing steels. The paper raises questions about the benefits that low Cr steels offer towards  
28 extending component design life compared to carbon steel under the test conditions considered  
29 here.

30 **Key words:** carbon dioxide, corrosion, X65, low-Cr steels, iron carbonate, chromium hydroxide

31 **1. Introduction**

32 Carbon capture and storage is considered as one of the main technologies available to assist  
33 in the abatement of climate change. The process has the potential to enable significant  
34 sequestration of high pressure carbon dioxide (CO<sub>2</sub>) in both depleted oil and gas fields and  
35 geological reservoirs. CO<sub>2</sub> injection can also be used for the purposes of enhanced oil recovery  
36 to extend the lifetime of oil and gas reservoirs.

37 Given the processes involved in CO<sub>2</sub> sequestration, corrosion of equipment can occur when  
38 large amounts of CO<sub>2</sub> in the dense phase are injected into storage sites. The injection pipeline  
39 receives compressed CO<sub>2</sub> typically in a liquid or supercritical state. When continuous injection  
40 is performed down a vertical line, water is displaced from the head of the pipeline. If the  
41 continuous process is ever interrupted, brine will proceed to flow back to the injection point,  
42 potentially rising hundreds of meters up the injection line before equilibrium is re-established<sup>[1]</sup>.  
43 Consequently, during this period the injection materials become exposed to a saline solution  
44 saturated with high pressure CO<sub>2</sub>. These sections of the line which are in contact with the CO<sub>2</sub>-  
45 containing brine can suffer particularly high levels of corrosion. Based on this, it is important to  
46 understand the corrosion severity under such static conditions and to select appropriate  
47 materials to ensure the integrity of the line for the duration of its intended operation.

48 The most cost-effective material for injection systems from the perspective of capital  
49 expenditure is carbon steel. However, this material is notoriously susceptible to CO<sub>2</sub> corrosion  
50 in the absence of protective corrosion products, making it prudent to also consider alternative  
51 materials to reduce operational expenditure if a particularly long design life is required <sup>[1, 2, 3]</sup>.  
52 Past research has highlighted the potential of low chromium (Cr) containing steels to offer  
53 improved strength, hardenability and corrosion resistance compared to carbon steel<sup>[4, 5, 6, 7]</sup>.  
54 These steels typically contain between 1 and 5% Cr and can provide a cost effective alternative  
55 compared to corrosion resistant alloys (CRAs)<sup>[5, 6, 7, 8, 9, 10, 11, 12, 13]</sup>. Kermani and Morshed<sup>[9]</sup>  
56 suggested that the use of 1-5Cr steel can improve the CO<sub>2</sub> corrosion resistance by a factor of  
57 2.5-40 with a cost penalty less than 1.5 times that of carbon steel.

58 There is a wealth of research reaching back to the 1980's<sup>[1, 7, 8, 10, 14, 15, 16, 17, 18, 19]</sup> focusing  
59 on the influence of 1-5% Cr addition to steels to improve strength, hardenability and CO<sub>2</sub>

60 corrosion resistance, with the majority of observations concluding that Cr addition does improve  
61 corrosion performance<sup>[7, 10]</sup>. In addition, a number of successful field trials have been reported<sup>[14,</sup>  
62 <sup>20]</sup> with the use of low Cr alloyed steels. However, a handful of researchers have identified  
63 adverse effects of Cr addition (i.e, a reduction in corrosion resistance of low alloyed steel with  
64 increasing Cr content) <sup>[14, 21, 22, 23]</sup> under specific operating conditions, presenting conflicting  
65 observations. Amit et al.,<sup>[23]</sup> reported 3Cr steel has a higher corrosion rate of 0.78 mm/year  
66 compared to the corrosion rate of 0.23 mm/year for 1Cr steel at 135°C.

67 One critical observation is the role of Cr-containing steel on influencing the chemistry,  
68 structure and morphology of corrosion products and how they contrast with corrosion products  
69 on carbon steels. In the majority of experiments, researchers have reported that corrosion rates  
70 begin to decline as protective corrosion products establish themselves<sup>[24, 25]</sup>. In simple CO<sub>2</sub>-  
71 containing brines with only sodium chloride (NaCl) as a dissolved salt, authors have reported  
72 the corrosion product iron carbonate (FeCO<sub>3</sub>) developing on carbon steel which assists in  
73 mitigating corrosion. However, for Cr-containing low alloy steels, the films can become enriched  
74 with undissolved Cr and some of its compounds, supposedly facilitating better general and  
75 localised corrosion protection<sup>[1, 16, 26, 27]</sup>. Researchers have also reported the development of  
76 duplex structures of the corrosion film on Cr-containing steels, consisting of an inner and outer  
77 layer<sup>[21, 26]</sup>. The Cr-enrichment of the inner film was believed to not only provide superior general  
78 and localised corrosion protection, but also assist in the prevention of local destruction of films  
79 by mechanically strengthening the corrosion product<sup>[21, 26]</sup>.

80 Despite an abundance of research into the potential advantages of low Cr alloyed steels,  
81 nearly all of the aforementioned studies have been conducted in environments at relatively low  
82 pressure where CO<sub>2</sub> exists in its gaseous state and conditions are more akin to what is seen in  
83 oil and gas transport, not in high pressure CO<sub>2</sub> injection. A few exceptions to this exist whereby  
84 Hassani et al.<sup>[15]</sup> evaluated the behaviour of 1018 carbon steel, 5Cr and 13Cr at 80 bar CO<sub>2</sub> and  
85 60°C and indicated that 5Cr was 3 times more corrosion resistant than carbon steel under such  
86 conditions, yet still produced a corrosion rate of 6 mm/year over 42 h of immersion. Pfennig et  
87 al.<sup>[28]</sup> also determined the corrosion resistance of 1Cr and 13Cr in both the brine and  
88 supercritical CO<sub>2</sub> phase at 100 bar and 60°C. Their research suggested that 1Cr was capable of  
89 handling the CO<sub>2</sub> stream conditions and the CO<sub>2</sub>-saturated brine phase, producing corrosion

90 rates comparable to 13Cr over 8000 h exposure, below 0.2 mm/year. However, no comparison  
91 was made with carbon steel, 3Cr or 5Cr under these specific conditions or across non-film  
92 forming conditions.

93 This paper addresses the knowledge gap in the area of low Cr alloy behaviour in **static** high  
94 pressure CO<sub>2</sub> environments by evaluating the corrosion response of four different steels (X65,  
95 1Cr, 3Cr and 5Cr) over time periods between 6 and 192 h at 60°C and 100 bar in a 1 wt.% NaCl  
96 solution. By examining all four materials, the influence of Cr content within the steel on the  
97 general and localised corrosion behaviour is investigated. The evolution, morphology and  
98 chemistry of corrosion products on the surface of each material are evaluated over time periods  
99 of 6, 24, 48, 96 and 192 h and related to the level of localised and general corrosion protection.  
100 In these experiments, a high surface area to volume ratio was deliberately chosen to generate  
101 significant film formation in a shorter timeframe. To understand the film formation  
102 characteristics, a combination of short duration and long duration experiments was performed.  
103 The focus of the short term (6 h) experiments was predominantly to understand the corrosion  
104 behaviour of the steels in the absence of protective corrosion products. These experiments can  
105 be thought of as more analogous to field conditions in an environment with a solution under-  
106 saturated with respect to various corrosion products. In longer duration tests, it is appreciated  
107 that a new set of equilibrium conditions become established at higher pH and greater Fe<sup>2+</sup>  
108 concentration in the bulk solution, which is a limitation of the closed system test methodology.  
109 However, the focus from long term experiments (192 h) is to determine the nature of the films  
110 developed when precipitation does occur and to evaluate the extent of protection they offer to  
111 the substrate in relation to both general and localised corrosion.

112 The experiments conducted within this paper attempt to simulate the process encountered  
113 during intermittent injection of CO<sub>2</sub>, whereby the brine rises back up the pipeline when injection  
114 ceases for a number of days. In this situation, a **static** fluid with a fixed volume is in contact with  
115 a specific internal area of pipeline.

## 116 **2. Experimental Procedure**

### 117 **2.1 Materials and Preparation**

118 All corrosion rates were measured based on gravimetric analysis of test specimens exposed  
119 to the brine solution for different durations between 6 and 192 h using a 1 L stainless steel  
120 autoclave. Mass loss specimens were machined from X65 carbon steel, 1Cr, 3Cr and 5Cr steel  
121 bars into discs of diameter 25 mm and thickness of 6 mm (an image of the prepared sample is  
122 embedded in Figure 1(a)). The chemical compositions of each of the materials considered are  
123 provided in Table 1. Surface preparation consisted of wet-grinding the entire sample surface  
124 with 600 grit silicon carbide (SiC) abrasive paper, rinsing with distilled water, followed by  
125 acetone, high purity ethanol and drying gently with compressed air. Samples were then stored  
126 in a desiccator until needed and weighed immediately before use on an electronic balance to  
127 within an accuracy of 0.01 mg before suspending inside the autoclave. Two samples were placed  
128 in the autoclave for each test, with experiments being repeated a minimum of 3 times.

## 129 **2.2 Microstructural characterisation**

130 Surface preparation for microstructural characterisation consisted of wet-grinding one  
131 sample surface up to 1200 grit SiC abrasive paper, followed by polishing using a polishing cloth  
132 with a 3  $\mu\text{m}$  diamond suspension to attain a mirror finish. Etchant concentration was varied  
133 depending on the sample alloy composition in accordance with in ASTM E3-01<sup>[29]</sup> and E407-99  
134 standards<sup>[30]</sup>. 2-5 % Nital solution was used for the different materials, with etching time varying  
135 from 10-20 seconds. Microstructural analysis was carried out using a LEICA DM 6000M upright  
136 optical microscope.

137 The microstructures of X65, 1Cr, 3Cr and 5Cr samples are presented in Figure 1. A ferritic-  
138 pearlitic microstructure is observed for X65 carbon steel. The microstructure of 3Cr shows  
139 carbides randomly distributed and the microstructure of 5Cr indicated carbides as dark areas in  
140 a ferrite matrix, while 1Cr shows an inhomogeneous distribution of martensite and ferrite.

## 141 **2.3 Mass loss tests**

142 A schematic representation of the autoclave experimental setup is provided in Figure 2 <sup>[31,</sup>  
143 <sup>32, 33]</sup>. The 1 wt.% NaCl solution used in each experiment was de-aerated by saturating the  
144 solution with CO<sub>2</sub> in a separate container for a minimum of 12 h prior to testing. The specimens  
145 were suspended within the autoclave using a non-conducting wire whilst also ensuring they  
146 were not in contact with the walls of the cylinder to prevent galvanic effects. The prepared, CO<sub>2</sub>-

147 saturated water was carefully delivered into the autoclave at ambient pressure and temperature  
148 and sealed. All lines to the autoclave were then purged with CO<sub>2</sub> and evacuated to ensure  
149 complete removal of oxygen within the system. The CO<sub>2</sub> was then transferred into the autoclave  
150 and heated and pressurised to the required temperature and pressure. The starting point of  
151 each test was taken from the time at which the autoclave reached the desired temperature and  
152 pressure of 60°C and 100 bar, respectively. Experiments for each material were conducted for  
153 6, 24, 48, 96 and 192 h to determine the changes in corrosion rate with time in **static** conditions.  
154 MultiScale<sup>[34]</sup> software was used to calculate the initial pH of the brine solution and was  
155 determined to be approximately 3.1 under the specified conditions.

156 Upon completion of each test, the specimens were dried thoroughly. They were then  
157 weighed and chemically cleaned to remove all traces of corrosion products before weighing  
158 again to determine the mass of corrosion product on the steel surface as well as the corrosion  
159 rate. The cleaning process consisted of wiping the surface with a cotton pad soaked in Clarke's  
160 solution (20 g antimony trioxide + 50 g stannous chloride + 1000 ml 38% hydrochloric acid) in  
161 accordance with ASTM Standard G1-03<sup>[35]</sup>. After cleaning, samples were rinsed with distilled  
162 water, followed by ethanol, before being dried with compressed air.

163 The mass loss due to corrosion was determined from the mass difference before exposure  
164 and after cleaning. The corrosion product mass is the difference before and after chemical  
165 cleaning, after exposure to the test environment.

166 The corrosion rates were calculated by using Equation (1):

$$V_c = \frac{87600\Delta m}{\rho AT} \quad (1)$$

167 Where  $V_c$  is the corrosion rate of the sample in mm/y,  $\Delta m$  is the mass loss in grams,  $\rho$  is the  
168 density of the sample in g/cm<sup>3</sup>,  $A$  is the exposed area in cm<sup>2</sup> and  $T$  is the immersion time in hours.

## 169 **2.4 Characterisation of corrosion products**

170 The surface coverage and morphology of the corrosion products were characterised using  
171 a Carl Zeiss EVO MA15 SEM. Raman spectroscopy was used to identify the nature of the

172 corrosion products locally on the surface and to detect the presence of potentially amorphous  
173 products not recorded by XRD.

## 174 **2.5 Interferometry**

175 Post-test profilometry measurements were performed on samples (scanning a 3 x 3 mm<sup>2</sup>  
176 area at a time) using a NP<sub>FLEX</sub> 3D Surface Metrology System to quantify localised attack. The  
177 objective used 10x magnification with approximately a 3.5 mm working distance. The pit depth  
178 analysis was conducted in alignment with ASTM Standard G46-94<sup>[36]</sup>. The standard stipulates  
179 that an average of the 10 deepest pits should be used for pit damage characterisation of the  
180 sample area.

## 181 **3 Results**

### 182 **3.1 The effect of steel Cr content on general corrosion rate in a CO<sub>2</sub>-saturated solution at** 183 **60°C and 100 bar**

184 Figure 3 presents the total mass loss and general corrosion rates of X65, 1Cr, 3Cr and 5Cr  
185 steel exposed to CO<sub>2</sub>-saturated 1 wt.% NaCl solution at 60°C and 100 bar for various immersion  
186 times from 6 and 192 h. Figure 3(a) expresses the mass loss as a function of time, while Figure  
187 3(b) indicates the average corrosion rates in mm/year for each material from 6 h to 192 h,  
188 assuming a uniform thickness loss over the steel surface.

189 Referring to Figure 3(b), during the initial 6 h, the highest corrosion rate of 16.6 mm/year  
190 was observed for X65 carbon steel. The general corrosion rate over the first 6 h for each material  
191 decreased as Cr content increased; the general corrosion rate for 5Cr was 6.7 mm/year, which  
192 was 2.5 times lower than X65 carbon steel. SEM images later in this paper indicate iron carbide  
193 (Fe<sub>3</sub>C) exposure due to the fast and selective dissolution of ferrite for X65. The images also  
194 indicate that the corrosion products on the carbon steel surface are minimal over this period.  
195 For the different Cr steels, a corrosion product layer was already evident on the steel surface  
196 after 6 h.

197 The general corrosion rates of X65, 1Cr, 3Cr and 5Cr steel over 192 h were 1.5, 1.9, 2.0 and  
198 2.1 mm/year, respectively. Despite the materials showing a clear benefit of higher Cr content  
199 during the initial 6 h, longer duration tests reflect that Cr addition has much less benefit in terms

200 of material dissolution, arguably demonstrating a negative effect on long-term corrosion  
201 behaviour in the closed system. This difference in corrosion rate is actually more significant than  
202 the 192 h average corrosion rates indicate. For example, by considering the time intervals and  
203 mass loss between 96 and 192 h in Figure 3(a), X65, 1Cr, 3Cr and 5Cr have corrosion rates of  
204 ~0.01, 0.10, 0.75 and 1.32 mm/year which is much more significant than the integrated  
205 corrosion rates represented in Figure 3(b).

206 The reduction in corrosion rates over the duration of 192 h for all samples is likely  
207 attributed to the formation of protective corrosion products on the steel surface. The following  
208 sections of this paper focus on identifying the key differences between the film structures,  
209 morphology and composition in an effort to understand the difference between the four  
210 materials in terms of their corrosion rates.

### 211 ***3.2 The influence of immersion time on corrosion product morphology – X65 and 5Cr***

212 The largest difference in general corrosion rate was observed for X65 and 5Cr as expected.  
213 Consequently the evolution of corrosion products on these two surfaces was studied in detail  
214 using SEM. Images of the top surface morphology formed on X65 carbon steel and 5Cr at various  
215 immersion times are shown in Figure 4, and the corresponding cross-sections featuring the  
216 thickness of corrosion products are provided in Figures 4 and 5.

217 After the first 6 h, a thin Fe<sub>3</sub>C layer of approximately 1 μm appeared on the X65 steel surface  
218 due to the high rate of ferrite dissolution (Figure 4(a)). (Confirmation of the revealing of this  
219 Fe<sub>3</sub>C layer is provided using XRD in our previous publication.<sup>[31]</sup>) Crystals then began to cover  
220 the steel surface after 24 h (shown in Figure 4(b)). Although the layer developed after 24 h was  
221 30 μm thick, gaps in the corrosion product were still visible where the electrolyte could easily  
222 access the steel substrate. After 96 h, a dense and more compact layer covered the entire  
223 surface and increased to a relatively uniform thickness of 60-65 μm. This layer contributed  
224 towards a reduction in corrosion rate. No significant change in the film morphology was  
225 observed beyond 96 h as shown in Figure 4(c) and 4(d).

226 To compare with the corrosion products formed on X65 carbon steel, Figure 4(e) – (h)  
227 presents the SEM top view images of 5Cr steel exposed to the CO<sub>2</sub>-saturated solution at 60°C and  
228 100 bar for various immersion times (with corresponding cross-sections in Figure 6). The SEM



229 images of the 5Cr steel surface showed a very different structure over the first 24 h of exposure  
230 compared to X65 steel. The images in Figures 4(e) and (f) feature a dehydrated/cracked,  
231 seemingly amorphous corrosion product film on the surface (based on cross-sections provided  
232 in Figures 6(a) to (c)). There was no difference in top view morphologies between 6 and 24 h,  
233 however, the thickness of the corrosion product layer increased from 1  $\mu\text{m}$  to 10  $\mu\text{m}$  (see Figures  
234 6(a) and (b)). It is clear from these images that the corrosion product which develops on the low  
235 Cr steel is generated very quickly and this may be responsible for its superior corrosion  
236 resistance compared to X65 in the early stages of corrosion. However, it is important to stress  
237 that although this amorphous film may result in a lower corrosion rate/mass loss compared to  
238 X65 over the first 24 h in Figure 3(a), the corrosion rate of 5Cr is still  $\sim 4.5$  mm/year between 6  
239 and 24 h based on mass loss values.

240 Crystals became visible under the SEM after 96 h exposure of 5Cr to the test solution (Figure  
241 4(g)), and were randomly distributed on top of the initially developed layer. After 192 h of  
242 exposure (Figure 4(h)) the corrosion product produced a two-layer structure and the formed  
243 crystals started to cover the entire surface. The thickness of the corrosion product layer  
244 measured approximately 60  $\mu\text{m}$  after 192 h, which was very similar to that of X65 at the same  
245 exposure time. However, in contrast to the crystalline film observed on X65 steel after 192 h,  
246 there are still identifiable gaps between crystals. Comparing the development of the crystals in  
247 Figures 4(f), (g) and (h) with the mass loss values for 5Cr in Figure 3(a), the rate of mass loss  
248 does not change significantly from 24 to 192 h. A relatively linear increase in mass loss is  
249 observed with time, despite the crystals clearly developing on the steel surface. This suggests  
250 that the inner amorphous layer is dictating the corrosion response of the steel surface, which is  
251 sensible given the crystals are not in direct contact with the substrate and appear not to present  
252 a particularly resistant diffusion barrier based on SEM analysis. Such behaviour contrasts with  
253 that of X65 steel under the same conditions where a more compact crystalline film has  
254 developed over the same time period.

### 255 ***3.3 Characterisation of two-layered corrosion product***

256 To understand the chemistry of the two-layered corrosion product, a combination of  
257 energy dispersive x-ray (EDX), XRD and Raman spectroscopy was employed. The EDX analysis of  
258 X65, 1Cr, 3Cr and 5Cr steel cross-sections and element distribution maps of the corrosion

259 product layers after 192 h of immersion are presented in Figure 7. The results show that the  
260 thickness of the corrosion products for X65, 1Cr, 3Cr and 5Cr are similar, reaching approximately  
261 60  $\mu\text{m}$  after 192 h exposure. Additionally, all samples display a duplex, or double layered  
262 structure comprising of an inner and outer layer. For X65 steel, the inner and outer layer  
263 chemical composition is very similar, comprising of mainly Fe, C and O. However, in the case of  
264 the Cr-containing steels, the inner layer contained significant levels of Cr, exhibiting a greater  
265 intensity in the EDX maps than that of the steel microstructure. This enrichment of Cr was  
266 particularly high at the interface between the inner and outer layer. Referring to Figure 3 and  
267 Figure 6, it is the formation of this inner Cr-rich layer on the low Cr-containing steels which  
268 contributes most towards the corrosion resistance and reduces the corrosion rates. In terms of  
269 the outer layers on the Cr-steels, only Fe, C, and O could be identified, with minimal Cr being  
270 detected.

271 To identify the nature of the corrosion product layers on different steel surfaces after 192  
272 h, XRD measurements were also conducted. The corresponding patterns provided in Figure 8  
273 showed that the only crystalline phase detected on all materials after 192 h was  $\text{FeCO}_3$  which  
274 relates to the crystals clearly visible on the outer layer. This observation agrees with the work  
275 done by Nazari et al.,<sup>[37]</sup> who indicated that  $\text{FeCO}_3$  formed on X70 samples exposed to 65°C and  
276 pH in the range of 5.5-6.5. No traces of crystalline Cr compounds within the corrosion product  
277 layer were detected on any of Cr-containing steels using XRD, indicating that the products are  
278 nano-crystalline or amorphous. This observation corroborates with the work of Guo et al.,<sup>[10]</sup>  
279 who showed through Transmission Electron Microscopy (TEM) analysis, that the inner layer of  
280 2Cr exposed to a  $\text{CO}_2$ -containing environment possessed an amorphous structure. Raman  
281 spectroscopy was used to further identify the inner film on both X65 and the low Cr steels. The  
282 spectra provided in Figure 9 relate to two scans conducted on 5Cr steel; one on the outer layer,  
283 and one on the inner layer which was analysed through the gaps present in the outer layer. The  
284 spectra are representative of the scans obtained on all three Cr-steels in that for the outer layer,  
285 three peaks located at 290, 743 and 1086  $\text{cm}^{-1}$  confirmed the presence of  $\text{FeCO}_3$  (blue spectra –  
286 Region A) and one peak located at 713  $\text{cm}^{-1}$  for the scan on the inner layer confirmed the  
287 presence of chromium hydroxide ( $\text{Cr}(\text{OH})_3$ ) (red spectra – Region B). In some spectra, traces of  
288  $\text{FeCO}_3$  (potentially amorphous or nano-crystalline) were also detected within the inner layer,  
289 though this mainly comprised of  $\text{Cr}(\text{OH})_3$ . Similar observations of  $\text{Cr}(\text{OH})_3$  have been reported

290 by Xu et al.,<sup>[6]</sup> who evaluated the corrosion behaviour of 1-6.5Cr steels in CO<sub>2</sub>-saturated  
291 formation water. They also reported that the inner amorphous layer is mainly comprised of  
292 Cr(OH)<sub>3</sub> by Raman analysis, with the detected main Cr(OH)<sub>3</sub> peak being observed at 713 cm<sup>-1</sup> by  
293 scanning Cr(OH)<sub>3</sub> powders. Similar conclusions were also made by Guo et al.,<sup>[10]</sup> who used TEM  
294 and XPS analysis to identify the inner layer of 2Cr steel and observed it is comprised of  
295 amorphous FeCO<sub>3</sub> and Cr(OH)<sub>3</sub>. Xu et al.<sup>[5]</sup> also studied the corrosion behaviour of 3Cr steel in  
296 CO<sub>2</sub>-saturated formation water at 80°C and 8 bar pCO<sub>2</sub> and have reported the same double layer  
297 structure consisting of a crystalline FeCO<sub>3</sub> layer on the top of an inner amorphous Cr-rich layer.

### 298 **3.4 Corrosion product mass and localised corrosion behaviour**

299 In addition to evaluating the role of corrosion product growth on the general corrosion  
300 behaviour, consideration is also afforded here to the propagation of pits on each steel surface  
301 as a function of time.

302 Surface profilometry measurements (examples provided in Figure 10) were performed  
303 after corrosion products were removed using Clarke's solution on every material after exposure  
304 to the test solution for 6, 24, 48, 96 and 192 h. Figure 11 shows the mass of the corrosion  
305 products formed on sample surfaces and the localised depth for X65, 1Cr, 3Cr and 5Cr steel  
306 exposed to CO<sub>2</sub>-saturated solution at 60°C and 100 bar for various immersion times.

307 For X65, the compact FeCO<sub>3</sub> layer provides protection against localised corrosion beyond  
308 96 h. However, 1Cr, 3Cr and 5Cr steels show higher localised attack which continues to  
309 propagate over the entire 192 h period. The localised depth of 1Cr, 3Cr and 5Cr exceeded that  
310 of X65, with 1Cr being the most susceptible to localised corrosion with a pit depth of 62 µm after  
311 192 h. Interestingly, the FeCO<sub>3</sub> inner layer on X65 steel suppresses pit propagation, while the  
312 inner layer which develops on 1Cr, 3Cr and 5Cr (which mainly comprises of Cr(OH)<sub>3</sub>) fails to fully  
313 suppress pit propagation over 192 h.

### 314 **3.5 Solution replenishment experiments to confirm film protective properties**

315 This research highlights that prior to the formation of a fully protective FeCO<sub>3</sub> layer on the  
316 steel surface, the corrosion resistance of the materials increased with increasing Cr content,  
317 agreeing with previous studies<sup>[7, 10]</sup>. However, an important message from this work is that as

318 the corrosion products grow over 192 h, the protection afforded to the different steels  
319 decreases with increasing Cr content. The results in Figure 3 show that X65 has the lowest  
320 corrosion rate after 192 hours exposure and 5Cr becomes the material with highest corrosion  
321 rate. The results also highlight the limitations of inferring corrosion behaviour of materials and  
322 their ranking based on experiments over individual fixed time intervals. For example, referring  
323 back to Figure 3, any single set of mass loss measurements at a particular time interval before  
324 96 h would produce the conclusion that increasing Cr content in the steel improves general  
325 corrosion resistance. However, extended tests performed in this work show this is not the case  
326 for this particular environment beyond 96 h if a corrosion product is capable of developing on  
327 the steel surface.

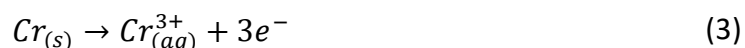
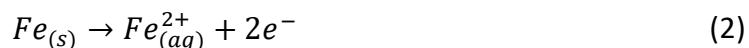
328 As discussed earlier in this paper, a limitation of the closed vessel experiment is the change  
329 in brine chemistry as a function of time and the consequences this has on the corrosion products  
330 formation as well as material corrosion behaviour. In order to address this issue and ensure the  
331 correct conclusions are made regarding the protectiveness of the corrosion products developed,  
332 solution replenishing was conducted after 48 h for X65 and 5Cr steel. At this instance in time, a  
333 fully formed  $\text{FeCO}_3$  layer was present on X65 steel (shown by the stable corrosion product mass  
334 in Figure 11(a)), while solely the amorphous  $\text{Cr}(\text{OH})_3$  layer was established on the 5Cr steel. The  
335 effect of solution replenishing is shown in Figure 12, which represents the average corrosion  
336 rate over 192 h. The results show that the films formed on X65 and 5Cr after 48 h are as  
337 protective as the 192 h data in Figure 3(b) suggests. This is important as the reduction in  
338 corrosion rate with time could be attributed to the change in solution chemistry, not the  
339 establishment of the film, and it is important to decouple these effects from one another to  
340 understand the true protectiveness of the developed corrosion products.

## 341 **4.0 Discussions**

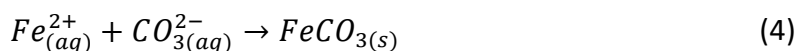
### 342 **4.1 Development of the duplex corrosion product**

343 The corrosion of carbon steel and low Cr steels in  $\text{CO}_2$ -containing brines is facilitated  
344 through the hydration of  $\text{CO}_2$  which produces carbonic acid ( $\text{H}_2\text{CO}_3$ ). The dissociation of  $\text{H}_2\text{CO}_3$   
345 in two steps produces the acidity ( $\text{H}^+$ ) within the aqueous phase.

346 The cathodic reactions of steel are related to the reduction of H<sup>+</sup> ions which are either  
347 supplied directly, or provided through the dissociation of H<sub>2</sub>CO<sub>3</sub> at the steel surface via a  
348 buffering effect<sup>[38]</sup>. The resulting anodic reactions are either the dissolution of iron, chromium,  
349 or both into the solution, depending on the material composition:



350 The formation of the corrosion products such as FeCO<sub>3</sub> and Cr(OH)<sub>3</sub> has been reported by  
351 several researchers in CO<sub>2</sub> environments<sup>[10, 39, 40]</sup> and occur when the products exceed their  
352 solubility locally within the system, resulting in precipitation onto the surface of the steel,  
353 typically via the following proposed processes:



354 Based on the corrosion product analysis described previously, a schematic representation  
355 of the corrosion product formation processes on the four steel surfaces is provided in Figure 13.  
356 With respect to X65 steel, the inner and outer layers begin to form at very similar times<sup>[31]</sup>, with  
357 the inner layer displaying less signs of crystallinity. However, from the perspective of the Cr  
358 steels, the inner amorphous layer (which is predominantly Cr(OH)<sub>3</sub>, with potential traces of  
359 amorphous/nano-crystalline FeCO<sub>3</sub>) clearly develops first. Once this layer reaches a critical level  
360 of protectiveness/thickness, it is followed by the precipitation of the outer crystalline FeCO<sub>3</sub>  
361 layer. Given the significant reduction in corrosion rate with time in the early stages of the Cr  
362 steels exposure, the majority, if not all of the protection is facilitated by the inner layer.

363 Furthermore, the Cr enrichment within the inner layer increases with the Cr content of the  
364 steel and this Cr-rich layer provides the corrosion protection, however, the protective nature of  
365 these layers in the context of general corrosion reduces with increasing steel Cr content.

366 The effect of Cr enrichment also appears to have implications for localised corrosion, with  
367 a higher pit depth being recorded after 192 h for the Cr steels compared to X65. The inner layer  
368 also appears to facilitate the continued growth of pits, partially aided by enabling easier access

369 of the electrolyte to the steel surface in comparison to the compact crystalline  $\text{FeCO}_3$  layer on  
370 the X65 steel surface. In contrast, the inner layer on X65 steel comprised solely of  $\text{FeCO}_3$  and  
371 was able to reduce the general corrosion rate the most effectively compare to the Cr steels,  
372 whilst also preventing the propagation of pits beyond 96 h of exposure.

373 Another key observation is the  $\text{FeCO}_3$  crystal size on the surfaces of the different steels.  
374 Increasing Cr content within the steel resulted in larger (and fewer)  $\text{FeCO}_3$  crystals forming  
375 within the outer layer (shown in Figure 4). The porosity of the outer layer visibly increases with  
376 Cr content in the steel, with an increase in crystal size and reduction in compactness. This  
377 correlates with the increase in general corrosion rate with Cr content, suggesting that the outer  
378 film may be responsible for providing some protection to the steel surface (although the  
379 majority of protection appears to be afforded by the inner layer in the case of the low Cr steels).

380 The larger, more discrete crystals at higher Cr content indicate a reduction in nucleation  
381 and enhanced growth with increasing Cr content in the steel. This can be explained by reviewing  
382 how the nucleation and growth characteristics change with the saturation ratio (SR) of  $\text{FeCO}_3$ ,  
383 which is essentially a measure of the extent to which the solubility limit is exceeded<sup>[28]</sup>:

$$384 \quad SR = \frac{[Fe^{2+}][CO_3^{2-}]}{K_{SP}} \quad (6)$$

385 where SR is the saturation ratio of  $\text{FeCO}_3$ ,  $[Fe^{2+}]$  and  $[CO_3^{2-}]$  are the concentrations of iron  
386 and carbonate ions in mol/L and  $K_{sp}$  is the solubility product for  $\text{FeCO}_3$  in  $\text{mol}^2/\text{L}^2$ .

387 The nucleation rate of  $\text{FeCO}_3$  varies exponentially with SR, while growth varies linearly.  
388 Consequently, high SR values result in high nucleation and less growth, while lower SR results in  
389 less nucleation and greater growth<sup>[24]</sup>. This suggests that the SR of the solution at the location  
390 of  $\text{FeCO}_3$  precipitation on the outer surface reduces as the Cr content in the steel increases. The  
391 growth of the outer film is also delayed as the Cr content in the steel increases. Both these  
392 observations correlate with the slower release of  $\text{Fe}^{2+}$  ions from the steel surface with increasing  
393 Cr content during the earlier stages of corrosion. As the  $\text{Fe}^{2+}$  flux from the surface reduces with  
394 increasing steel Cr content (due to the suppression of corrosion rate from the  $\text{Cr}(\text{OH})_3$  film), the  
395 solution will take longer to become saturated with respect to  $\text{FeCO}_3$  and will not reach as high  
396 values of SR, resulting in the development of larger, more discrete crystals within the outer layer.

## 397 **6 Conclusions**

398 In this work, the corrosion behaviour of X65, 1Cr, 3Cr and 5Cr steel exposed to CO<sub>2</sub>-  
399 saturated 1 wt.% NaCl brine at 60°C and 100 bar for various immersions times was studied. The  
400 findings from this work are as follows:

- 401 1. In the early stages of corrosion, in the absence of significant corrosion product formation,  
402 the general corrosion rate of X65 exhibited the highest corrosion rate (16.7 mm/year).  
403 Corrosion resistance of the four materials increased with increasing Cr content (corrosion  
404 resistance: X65<1Cr<3Cr<5Cr), the presence of low Cr content (1-5%) produced a  
405 chromium hydroxide (Cr(OH)<sub>3</sub>) film in the first 6 h of exposure to the test solution.  
406 Increasing Cr content within the steel proved beneficial toward mitigating material  
407 dissolution in the absence of formation of protective corrosion products, suppressing  
408 corrosion rate by a factor of 2.5 for 5Cr steel over the first 6 h.
- 409 2. Longer durations of exposure for all materials resulted in the formation of protective  
410 corrosion products consisting of a duplex structure (an inner amorphous/nano-  
411 crystalline layer and an outer crystalline layer). The outer layer on all samples comprised  
412 of solely FeCO<sub>3</sub>. The inner layer for X65 consisted of FeCO<sub>3</sub> only, while for Cr steel,  
413 contained significant levels of Cr enrichment as a result of Cr(OH)<sub>3</sub> presence, as well as  
414 trace amounts of FeCO<sub>3</sub>.
- 415 3. After 192 h of exposure, the thickness of the corrosion products were very similar (60  
416 µm), but offered different levels of protection against general and localised corrosion.  
417 The Cr enrichment of the inner film appeared to facilitate continued pit propagation,  
418 with a reduction in general corrosion protection being observed with increasing Cr  
419 content in the steel and the film.
- 420 4. The corrosion product layer formed on X65 steel after 192 h was able to significantly  
421 suppress general corrosion (corrosion resistance: X65>1Cr>3Cr>5Cr). The extent of  
422 localised corrosion decreased significantly for X65 as it became covered by dense and  
423 compact FeCO<sub>3</sub> compared to the Cr-containing steels, and increasing Cr content failed to  
424 improve localised corrosion resistance.
- 425 5. The presence of Cr in the steels influenced the nucleation and growth characteristics of  
426 FeCO<sub>3</sub> crystals on the outer layer which was predominantly due to the rate of release of

427 Fe<sup>2+</sup> ions into the solution in the earlier stages of corrosion, resulting in different  
428 saturation ratios at the location of FeCO<sub>3</sub> precipitation.

429 6. The work also highlighted that individual mass loss tests at a specific time intervals can  
430 result in the misinterpretation of material corrosion resistance ranking when protective  
431 corrosion products develop on steel surfaces. Multiple experiments over the film  
432 formation period are required to fully characterise material behaviour in the presence of  
433 such films to produce reliable conclusions regarding the protection afforded by corrosion  
434 products. The results indicate that the low Cr steels are no more suitable for this situation  
435 compared to X65 carbon steel under the tests conditions considered here.

436

### 437 **5. References**

- 438 1. Ikeda, A., M. Ueda, and S. Mukai, CO<sub>2</sub> Behavior of Carbon and Chromium Steels.(Retroactive  
439 Coverage). Advances in CO<sub>2</sub> Corrosion., 1984. 1: p. 39-51.
- 440 2. J. Crolet, N. Thevenot, and S. Netic, Role of Conductive Corrosion Products in the  
441 Protectiveness of Corrosion Layers. Corrosion, 1998. 54(3): p. 194-203.
- 442 3. S. Netic and L. Lunde, Carbon dioxide corrosion of carbon steel in two-phase flow. Corrosion,  
443 1994. 50(9): p. 717-727.
- 444 4. E.P. DeGarmo, J.T. Black, R.A. Kohser, and B.E. Klamecki, Materials and process in  
445 manufacturing. 1997: Prentice Hall.
- 446 5. L.N. Xu, S.Q. Guo, W. Chang, T.H. Chen, L.H. Hu, and M.X. Lu, Corrosion of Cr bearing low  
447 alloy pipeline steel in CO<sub>2</sub> environment at static and flowing conditions. Applied Surface  
448 Science, 2013. 270: p. 395-404.
- 449 6. L. Xu, B. Wang, J. Zhu, W. Li, and Z. Zheng, Effect of Cr content on the corrosion performance  
450 of low-Cr alloy steel in a CO<sub>2</sub> environment. Applied Surface Science, 2016. 379: p. 39-46.
- 451 7. J. Sun, C. Sun, and Y. Wang, Effect of Cr Content on the Electrochemical Behavior of Low-  
452 chromium X65 Steel in CO<sub>2</sub> Environment. Int. J. Electrochem. Sci, 2016. 11: p. 8599-8611.
- 453 8. C. Chen, M. Lu, D. Sun, Z. Zhang, and W. Chang, Effect of chromium on the pitting resistance  
454 of oil tube steel in a carbon dioxide corrosion system. Corrosion, 2005. 61(6): p. 594-601.
- 455 9. M.B. Kermani and A. Morshed, Carbon Dioxide Corrosion in Oil and Gas Production - A  
456 Compendium. Corrosion, 2003. 59(8): p. 659-683.
- 457 10. S.Q. Guo, L.N. Xu, L. Zhang, W. Chang, and M.X. Lu, Corrosion of Alloy Steels Containing 2%  
458 Chromium in CO<sub>2</sub> Environments. Corrosion Science, 2012. 63: p. 246-258.

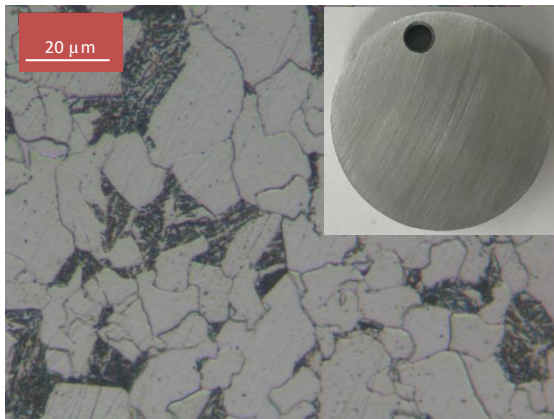


- 459 11. R. Barker, Y. Hua, and A. Neville, Internal corrosion of carbon steel pipelines for dense-phase  
460 CO<sub>2</sub> transport in carbon capture and storage (CCS)—a review. *International Materials Reviews*,  
461 2017. 62(1): p. 1-31.
- 462 12. J.B. Sun, W. Liu, W. Chang, Z.H. Zhang, Z.T. Li, T. Yu, and M.X. Lu, Characteristics and  
463 formation mechanism of corrosion scales on low-chromium X65 steels in CO<sub>2</sub> environment.  
464 *Acta Metall Sin*, 2009. 45(1): p. 84.
- 465 13. J. Sun, C. Sun, X. Lin, X. Cheng, and H. Liu, Effect of chromium on corrosion behavior of P110  
466 steels in CO<sub>2</sub>-H<sub>2</sub>S environment with high pressure and high temperature. *Materials*, 2016.  
467 9(3): p. 200.
- 468 14. K. Nose, H. Asahi, P. I. Nice, and J. W. Martin. Corrosion properties of 3% Cr steels in oil and  
469 gas environments. in *CORROSION 2001*. 2001. NACE International.
- 470 15. S. Hassani, T.N. Vu, N.R. Rosli, S.N. Esmaeely, Y.-S. Choi, D. Young, and S. Nestic, Wellbore  
471 integrity and corrosion of low alloy and stainless steels in high pressure CO<sub>2</sub> geologic storage  
472 environments: An experimental study. *International Journal of Greenhouse Gas Control*,  
473 2014. 23: p. 30-43.
- 474 16. T. Muraki, T. Hara, and H. Asahi. Effects of chromium content up to 5% and dissolved oxygen  
475 on CO<sub>2</sub> corrosion. in *CORROSION 2002*. 2002. NACE International.
- 476 17. S. Zhang, L. Hou, Y. Wei, H. Du, H. Wei, B. Liu, and X. Chen, Dual functions of chloride ions  
477 on corrosion behavior of mild steel in CO<sub>2</sub> saturated aqueous solutions. *Materials and*  
478 *Corrosion*.
- 479 18. S. Zhang, L. Hou, H. Wei, Y. Wei, and B. Liu, Failure analysis of an oil pipe wall perforated by  
480 pitting corrosion. *Materials and Corrosion*, 2018. 69(8): p. 1123-1130.
- 481 19. L. Hou, M. Raveggi, X.-B. Chen, W. Xu, K.J. Laws, Y. Wei, M. Ferry, and N. Birbilis. Investigating  
482 the passivity and dissolution of a corrosion resistant Mg-33at.% Li alloy in aqueous chloride  
483 using online ICP-MS. *Journal of The Electrochemical Society* 2016 [cited 163 6]; C324-C329].
- 484 20. B. Kermani, J.C. Gonzales, G.L. Turconi, T.E. Perez, and C. Morales. In-field corrosion  
485 performance of 3% Cr steels in sweet and sour downhole production and water injection. in  
486 *CORROSION 2004*. 2004. NACE International.
- 487 21. A. Dugstad, H. Hemmer, and M. Seiersten, Effect of steel microstructure on corrosion rate  
488 and protective iron carbonate film formation. *Corrosion*, 2001. 57(4): p. 369-378.

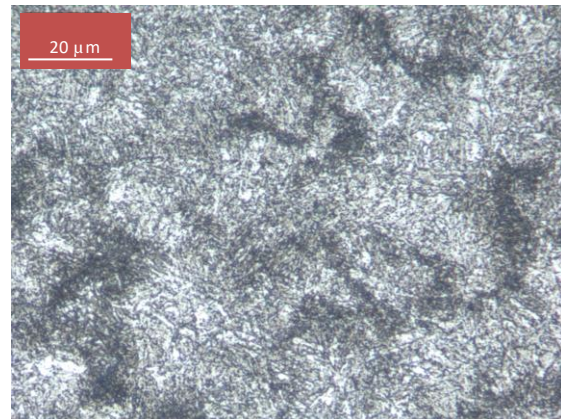
- 489 22. B. Kermani, M. Dougan, J.C. Gonzalez, C. Linne, and R. Cochrane. Development of low carbon  
490 Cr-Mo steels with exceptional corrosion resistance for oilfield applications. in CORROSION  
491 2001. 2001. NACE International.
- 492 23. A. Kumar, S.K. Desai, J.L. Pacheco, W. Sun, W. Huang, and M. Asmann. Corrosion  
493 Performance of L80-1Cr and L80-3Cr Oil Country Tubular Goods (OCTG) in High CO<sub>2</sub> at  
494 Elevated Temperature. in CORROSION 2013. 2013. NACE International.
- 495 24. R. Elgaddafi, A. Naidu, R. Ahmed, S. Shah, S. Hassani, S.O. Osisanya, and A. Saasen, Modeling  
496 and experimental study of CO<sub>2</sub> corrosion on carbon steel at elevated pressure and  
497 temperature. Journal of Natural Gas Science and Engineering, 2015. 27: p. 1620-1629.
- 498 25. Y. Hua, A. Shamsa, R. Barker, and A. Neville, Protectiveness, morphology and composition of  
499 corrosion products formed on carbon steel in the presence of Cl<sup>-</sup>, Ca<sup>2+</sup> and Mg<sup>2+</sup> in high  
500 pressure CO<sub>2</sub> environments. Applied Surface Science, 2018. 455: p. 667-682.
- 501 26. M. Ueda and H. Takabe. The formation behavior of corrosion protective films of low Cr  
502 bearing steels in CO<sub>2</sub> environments. in CORROSION 2001. 2001. NACE International.
- 503 27. Y. Xiang, H. Huang, Z. Long, C. Li, and W. Yan, Role of residual 2-amino-2-methyl-1-propanol  
504 and piperazine in the corrosion of X80 steel within an impure supercritical CO<sub>2</sub> environment  
505 as relevant to CCUS. International Journal of Greenhouse Gas Control, 2019. 82: p. 127-137.
- 506 28. A. Pfennig and R. Bäßler, Effect of CO<sub>2</sub> on the stability of steels with 1% and 13% Cr in saline  
507 water. Corrosion Science, 2009. 51(4): p. 931-940.
- 508 29. ASTM, E3-01. 2002: Standard Practice for Preparation of Metallographic Specimens. Annual  
509 Book of ASTM Standards, ASTM.
- 510 30. ASTM, E 407-99, Standard Guide for Microetching Metals and Alloys. American Society for  
511 Testing Materials.
- 512 31. Y. Hua, R. Barker, and A. Neville, Comparison of corrosion behaviour for X-65 carbon steel in  
513 supercritical CO<sub>2</sub>-saturated water and water-saturated/unsaturated supercritical CO<sub>2</sub> The  
514 Journal of Supercritical Fluids, 2015. 97: p. 224-237.
- 515 32. Y. Hua, R. Barker, and A. Neville, Effect of temperature on the critical water content for  
516 general and localised corrosion of X65 carbon steel in the transport of supercritical CO<sub>2</sub>. The  
517 International Journal of Greenhouse Gas Control, 2014. 31: p. 48-60.
- 518 33. Y. Hua, R. Barker, C. T. M. Ward, and A. Neville, Relating Iron Carbonate Morphology to  
519 Corrosion Characteristics for Water-Saturated Supercritical CO<sub>2</sub> Systems. The Journal of  
520 Supercritical Fluids, 2014. vol. 98: p. 183-193.

- 521 34. MultiScale 7.1 is a commercial software package from Expro Group International Ltd, for  
522 more information see: <http://multiscale.no/>.
- 523 35. ASTM, Standard G1-03, Standard practice for preparing, cleaning, and evaluating corrosion  
524 test specimens. ASTM International: West Conshohocken, PA, 2003.
- 525 36. ASTM, Standard G46-94, Standard guide for examination and evaluation of pitting corrosion.  
526 ASTM International: West Conshohocken, PA, 2003.
- 527 37. M.H. Nazari, S. Allahkaram, and M. Kermani, The effects of temperature and pH on the  
528 characteristics of corrosion product in CO<sub>2</sub> corrosion of grade X70 steel. Materials & Design,  
529 2010. 31(7): p. 3559-3563.
- 530 38. A. Dugstad, Mechanism of Protective Film Formation During CO<sub>2</sub> Corrosion of Carbon Steel,  
531 in CORROSION 981998, NACE International: Sand Diego, CA:NACE.
- 532 39. W. Sun and S. Nescic, Basics revisited: kinetics of iron carbonate scale precipitation in CO<sub>2</sub>  
533 corrosion. Corrosion/2006, paper, 2006(06365).
- 534 40. A. Dugstad, The importance of FeCO<sub>3</sub> supersaturation on the CO<sub>2</sub> corrosion of mild steels.  
535 CORROSION/92, paper, 1992(14).

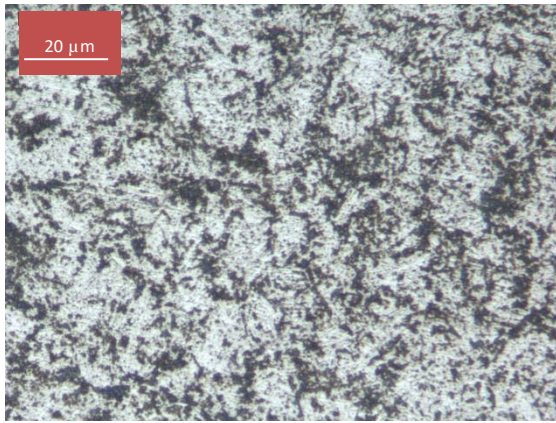
536



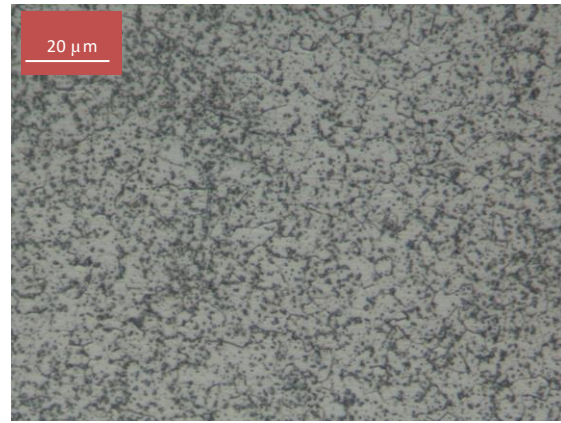
(a)



(b)



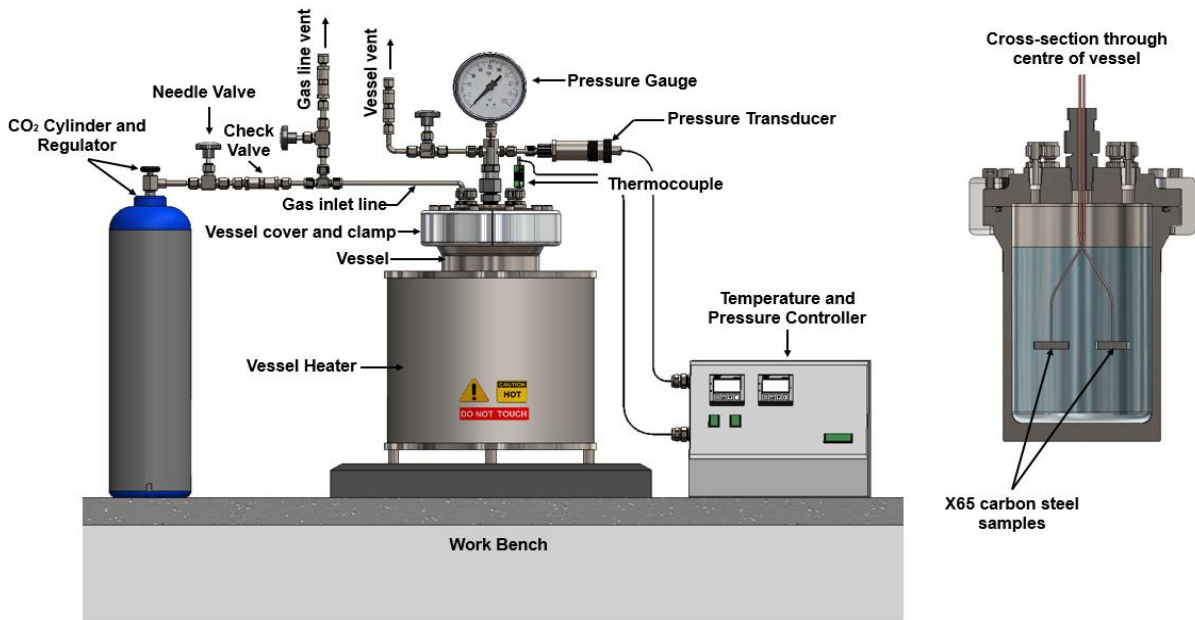
(c)



(d)

537  
538

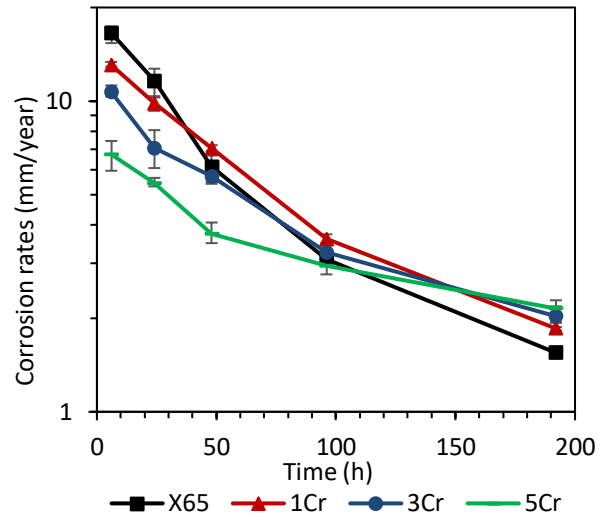
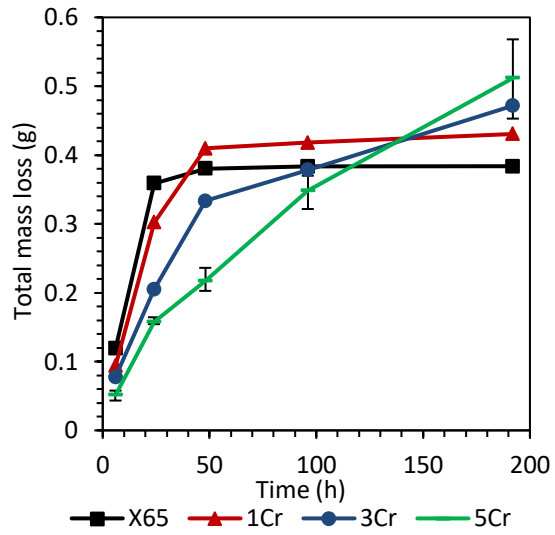
**Figure 1: Optical microscope images of microstructures for (a) X65, (b) 1Cr, (c) 3Cr and (d) 5Cr. Note: A typical sample coupon is shown in the insert in (a).**



539

540

**Figure 2: Schematic of autoclave setup**



541

542

543

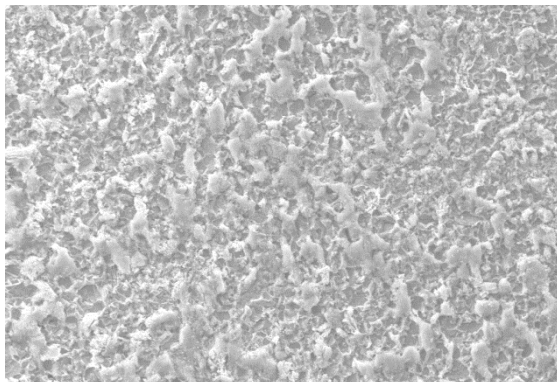
544

545

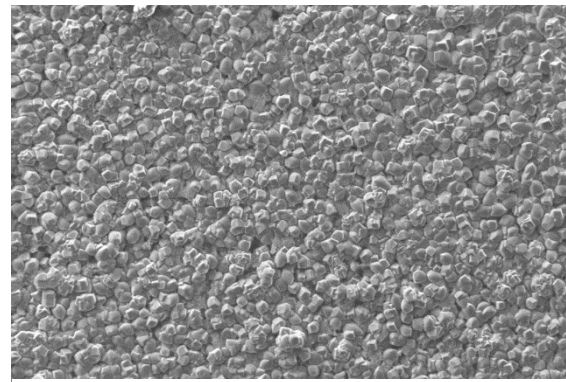
(a)

(b)

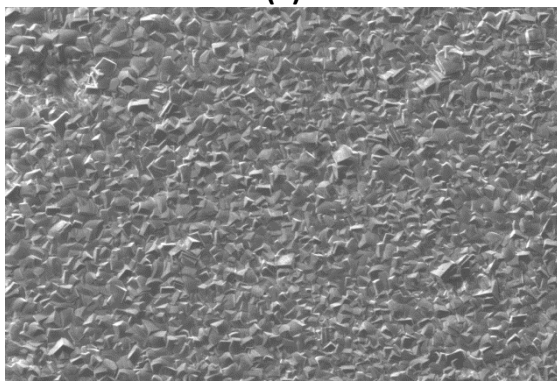
**Figure 3: Plots depicting (a) total mass loss and (b) general corrosion rates for X65, 1Cr, 3Cr and 5Cr steel exposed to a CO<sub>2</sub>-saturated 1 wt.% NaCl solution at various immersion times at 60°C and 100 bar**



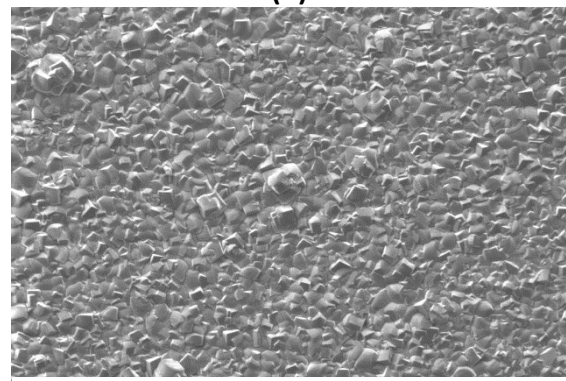
Mag = 464 X 20.00 kV SE1 100  
**(a)**



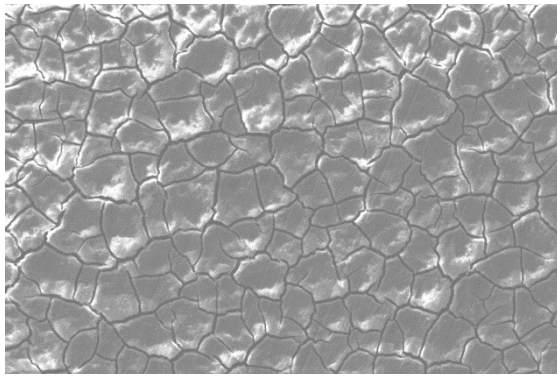
Mag = 464 X 20.00 kV SE1 100  
**(b)**



Mag = 464 X 20.00 kV SE1 100  
**(c)**

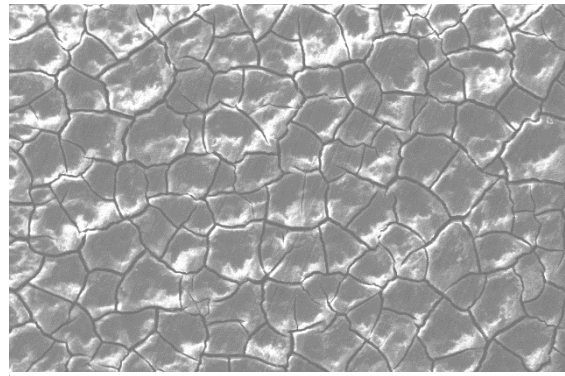


Mag = 464 X 20.00 kV SE1 100  
**(d)**



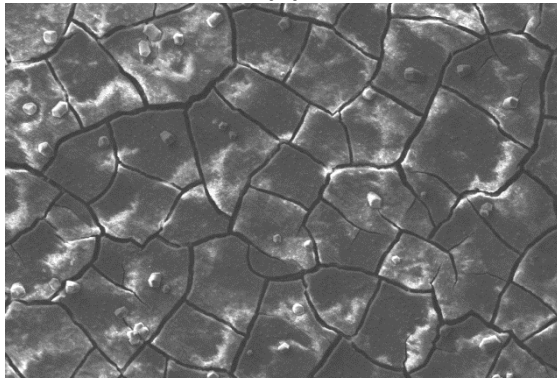
Mag = 464 X 20.00 kV SE1 100

(e)



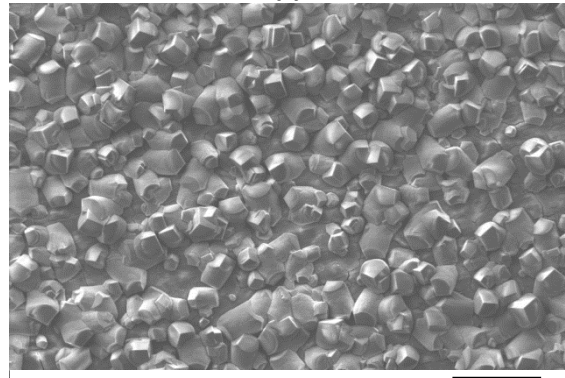
Mag = 464 X 20.00 kV SE1 100

(f)



Mag = 464 X 20.00 kV SE1 100

(g)

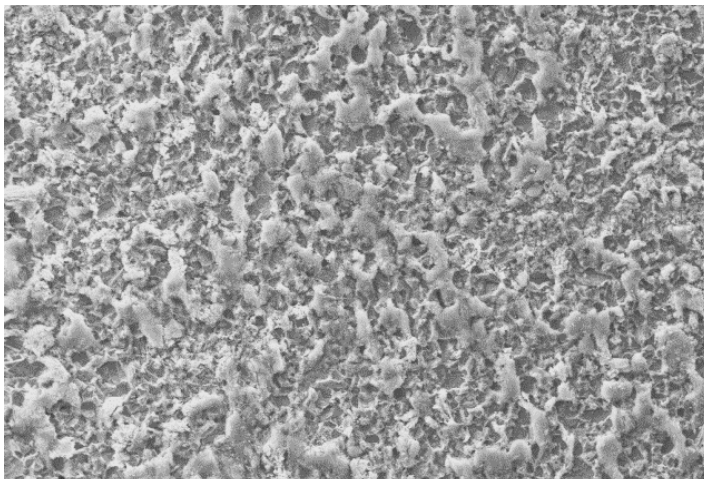


Mag = 464 X 20.00 kV SE1 100

(h)

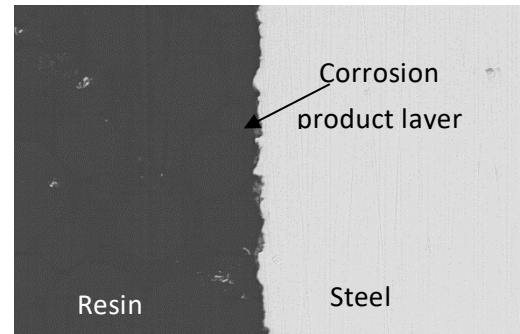
546 **Figure 4: SEM images of surface morphology of corrosion products formed on X65 exposed**  
 547 **to a CO<sub>2</sub>-saturated 1 wt.% NaCl solution at 60°C and 100 bar for various immersion periods of**  
 548 **(a) 6 h, (b) 24 h, (c) 96 h and (d) 192 h. The corrosion products for 5Cr exposed to a CO<sub>2</sub>-**  
 549 **saturated 1 wt.% NaCl solution at 60°C and 100 bar for immersion periods of (e) 6 h, (f) 24 h,**  
 550 **(g) 96 h and (h) 192 h. The corresponding cross-sections are provided in Figures 5 and 6.**

551

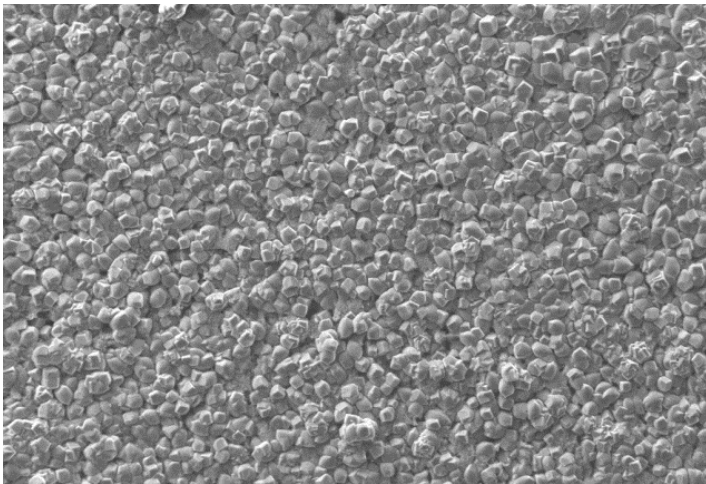


Mag = 464 X 20.00 kV SE1 100 μm

(a)

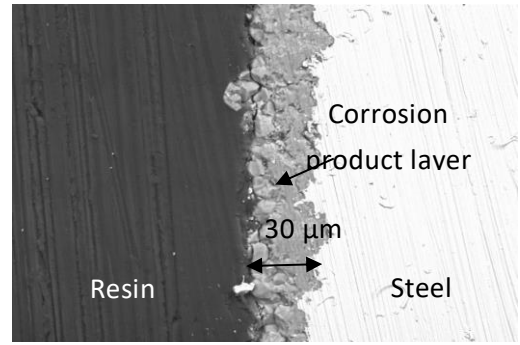


Mag = 1.00 KX 20.00 kV SE1 10 μm

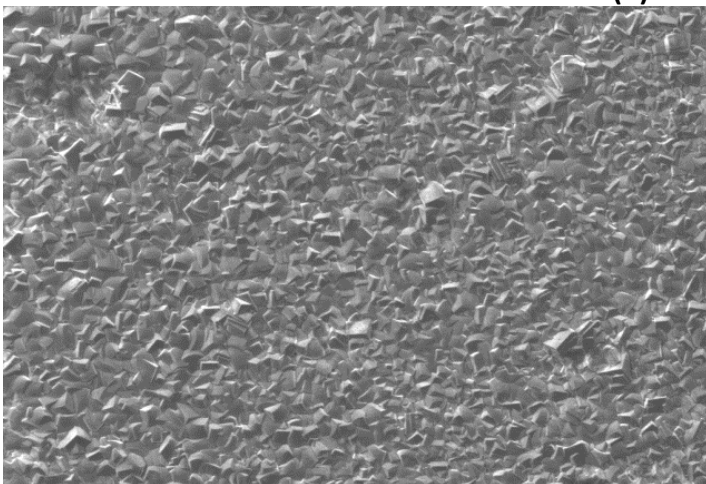


Mag = 464 X      20.00 kV      SE1      100 μm

(b)

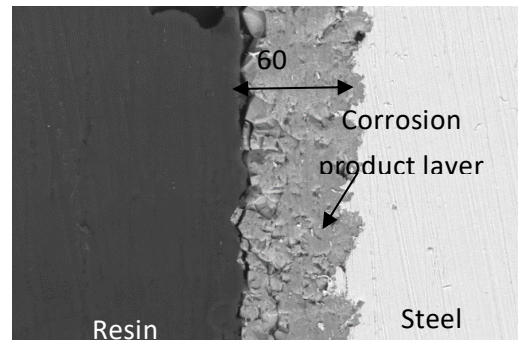


Mag = 1.00 KX      20.00 kV      SE1      10 μm

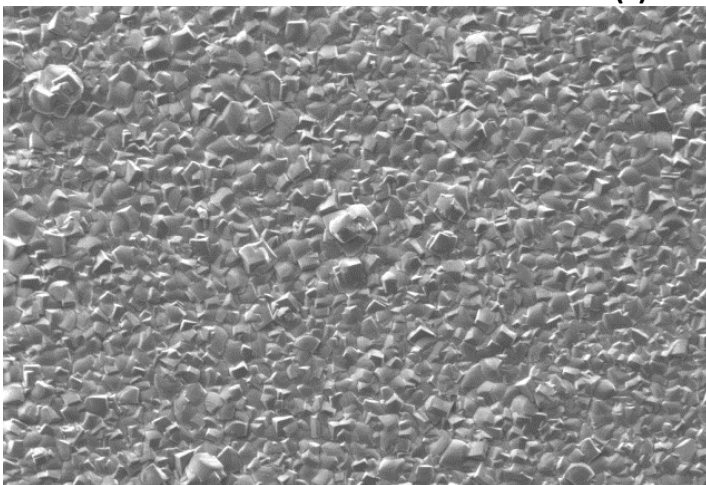


Mag = 464 X      20.00 kV      SE1      100 μm

(c)

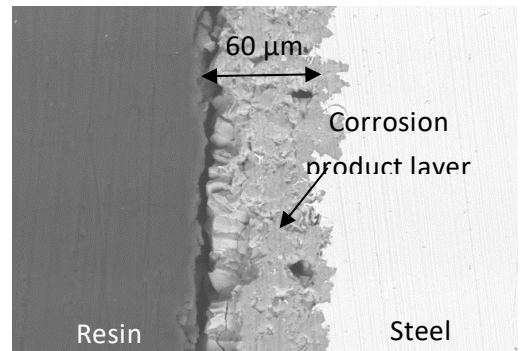


Mag = 1.00 KX      20.00 kV      SE1      10 μm



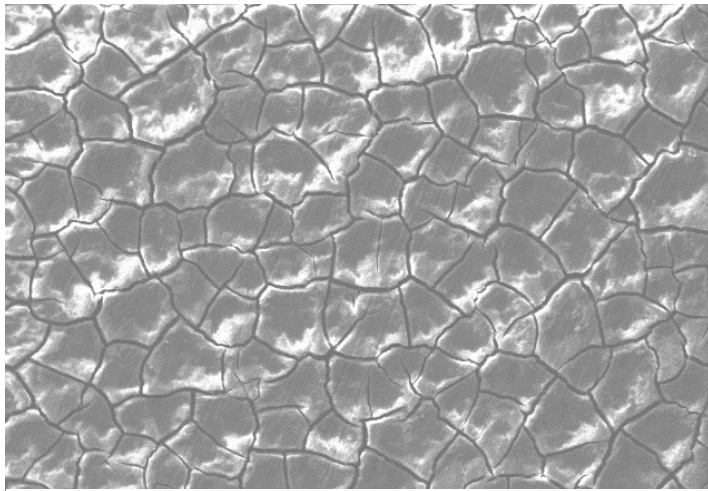
Mag = 464 X      20.00 kV      SE1      100 μm

(d)

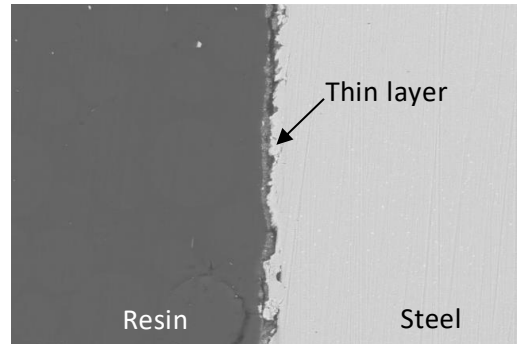


Mag = 1.00 KX      20.00 kV      SE1      10 μm

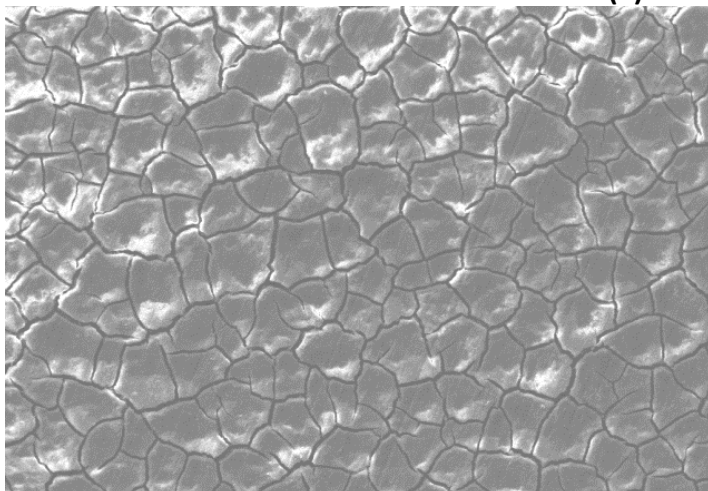
552 **Figure 5: SEM images of surface morphology and corresponding cross sections of corrosion**  
 553 **products formed on X65 carbon steel exposed to a CO<sub>2</sub>-saturated 1 wt.% NaCl solution at**  
 554 **60°C and 100 bar for various immersion periods of (a) 6 h, (b) 24 h, (c) 96 h and (d) 192 h.**  
 555



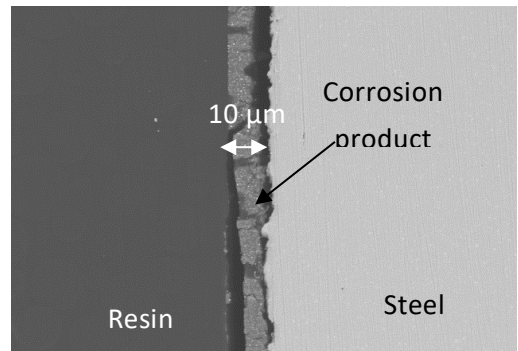
Mag = 464 X      20.00 kV      SE1      100  $\mu$ m  
**(a)**



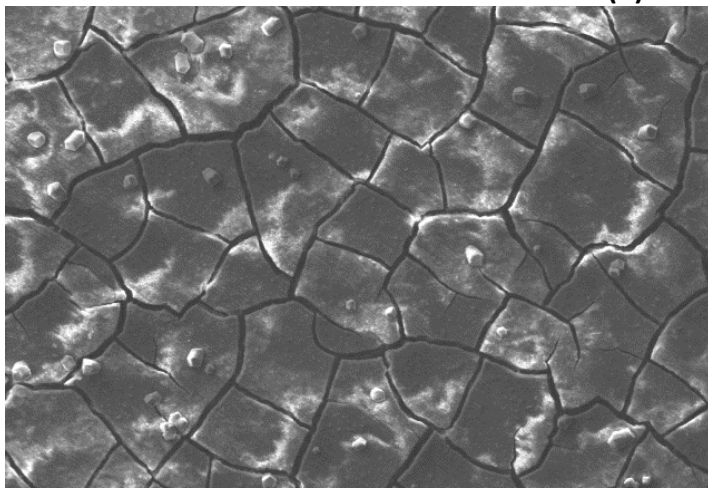
Mag = 1.00 KX      20.00 kV      SE1      10  $\mu$ m



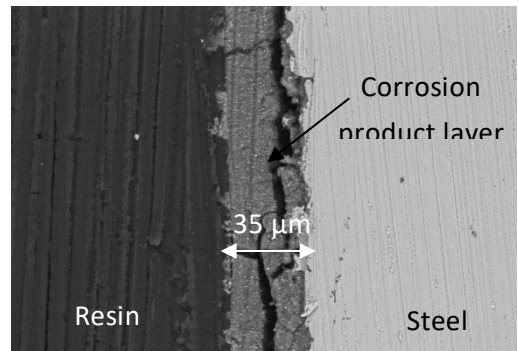
Mag = 464 X      20.00 kV      SE1      100  $\mu$ m  
**(b)**



Mag = 1.00 KX      20.00 kV      SE1      10  $\mu$ m

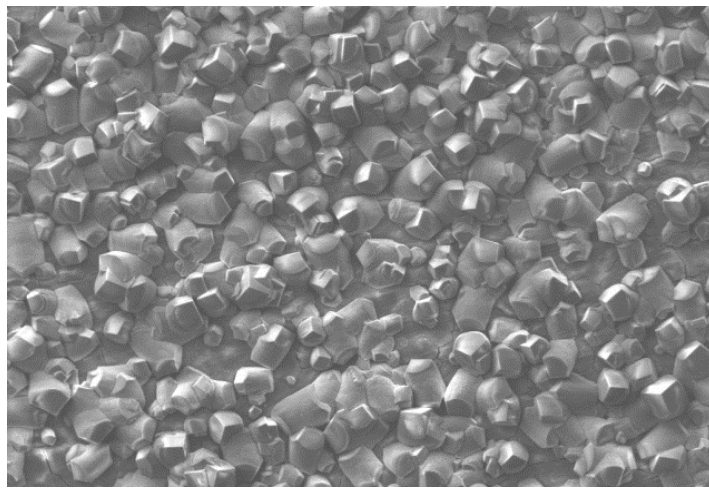


Mag = 464 X      20.00 kV      SE1      100  $\mu$ m  
**(c)**



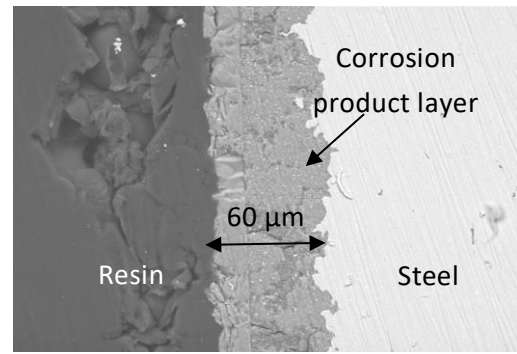
Mag = 1.00 KX      20.00 kV      SE1      10  $\mu$ m





Mag = 464 X      20.00 kV      SE1      100 μm

(d)



Mag = 1.00 KX      20.00 kV      SE1      10 μm

556 **Figure 6: SEM images of surface morphology and corresponding cross sections of corrosion**  
557 **products formed on 5Cr steel exposed to a CO<sub>2</sub>-saturated 1 wt.% NaCl solution at 60°C and**  
558 **100 bar for various immersion periods of (a) 6 h, (b) 24 h, (c) 96 h and (d) 192 h.**  
559

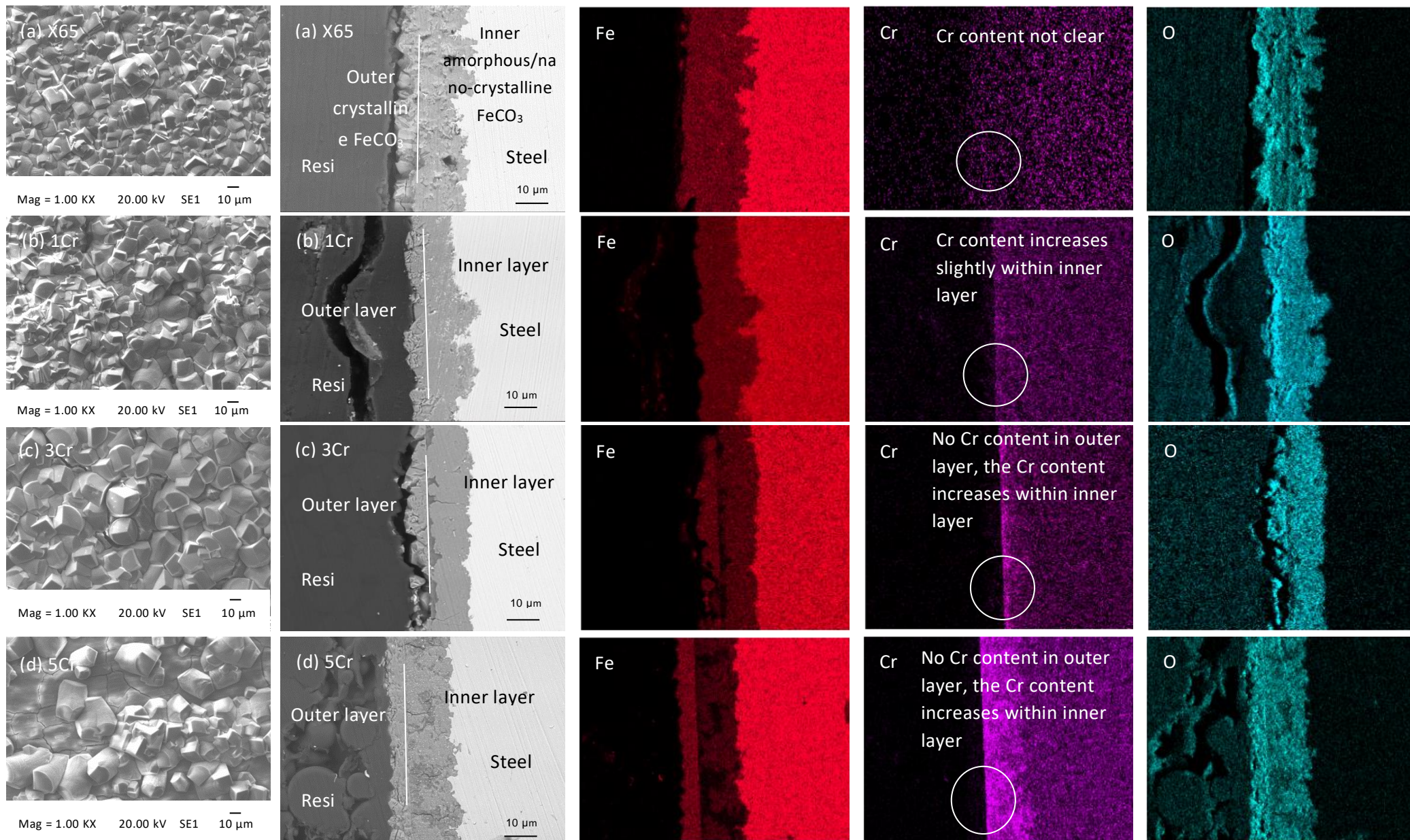
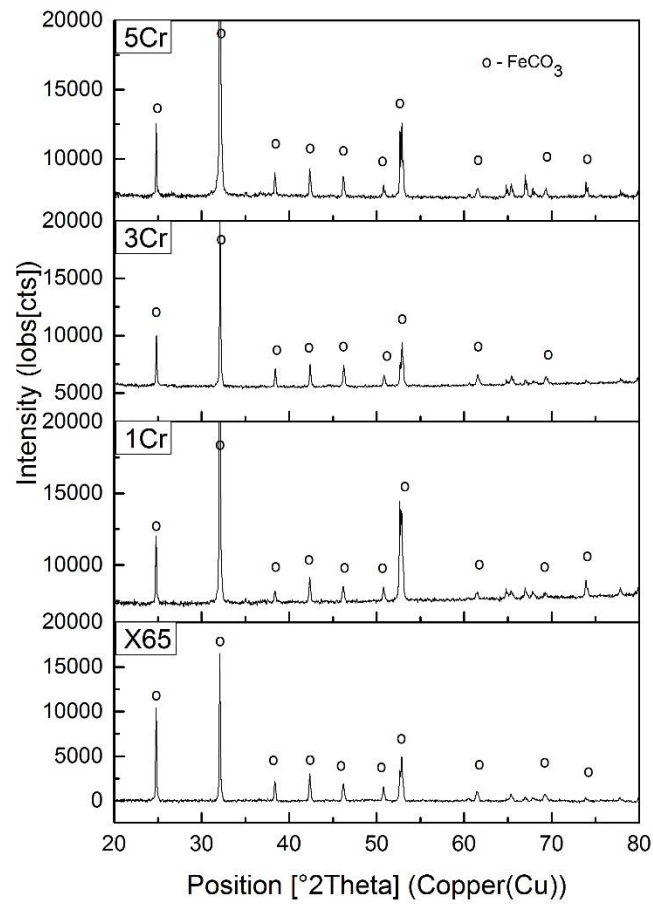


Figure 7: SEM cross-section images and EDX maps of (a) X65, (b) 1Cr, (c) 3Cr and (d) 5Cr samples exposed to CO<sub>2</sub>-saturated solution at 100 bar and 60°C for 192 h.



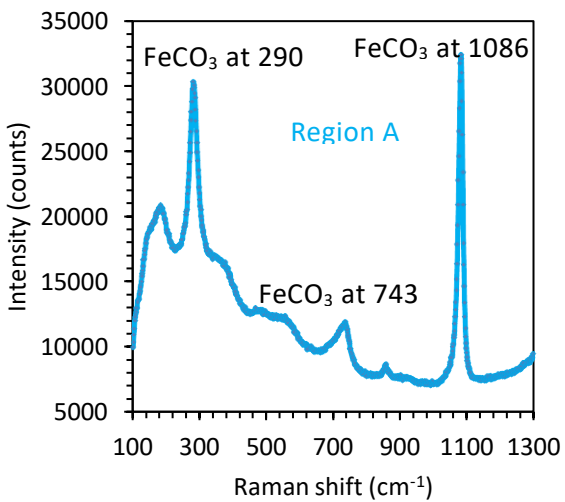
562

563 **Figure 8: XRD patterns of X65, 1Cr, 3Cr and 5Cr samples exposed to a CO<sub>2</sub>-saturated 1 wt.%**  
 564 **NaCl solution at 100 bar and 60°C for 192 h.**

565

566

567



568

569

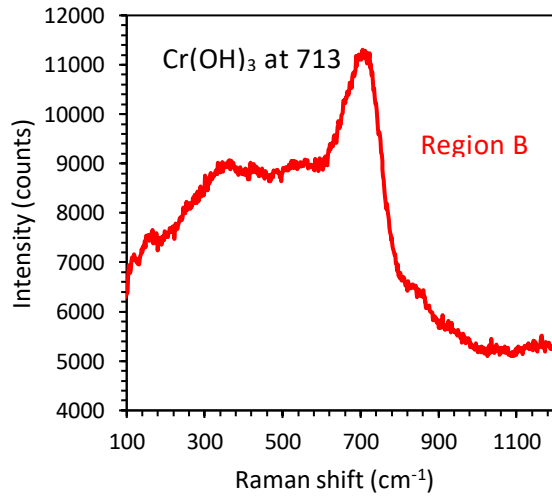
570

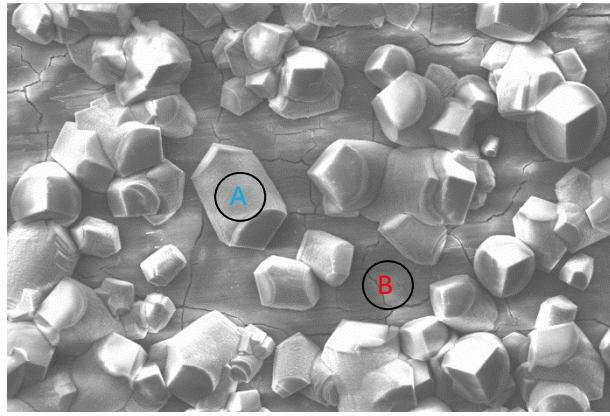
571

572

573

574



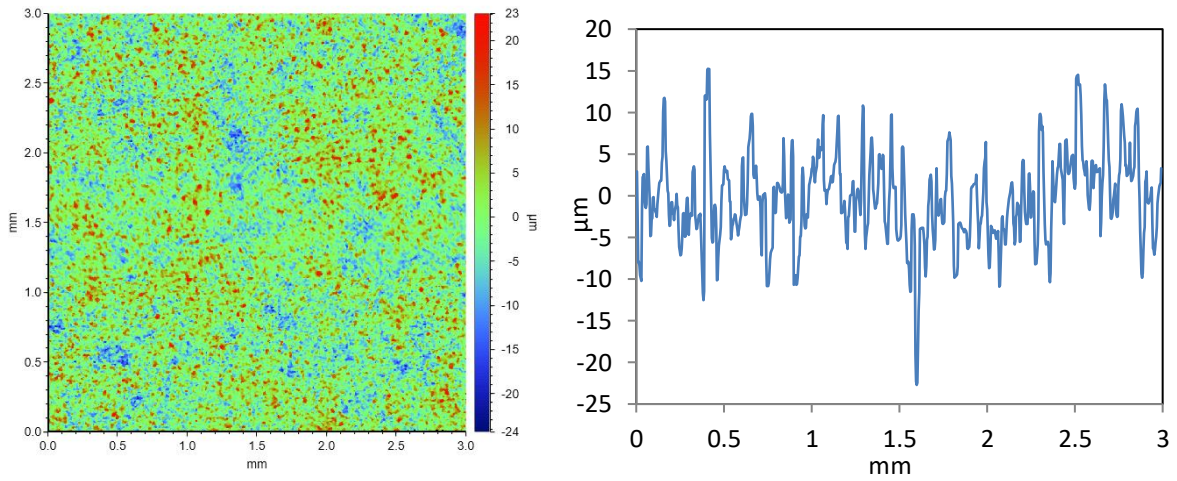


Mag = 1.00 KX      20.00 kV      SE1      10 μm

575

576 **Figure 9: Raman spectroscopy of the corrosion products at particular positions from 5Cr steel**  
 577 **exposed to a CO<sub>2</sub>-saturated 1 wt.% NaCl solution at 60°C and 100 bar for 192 h**

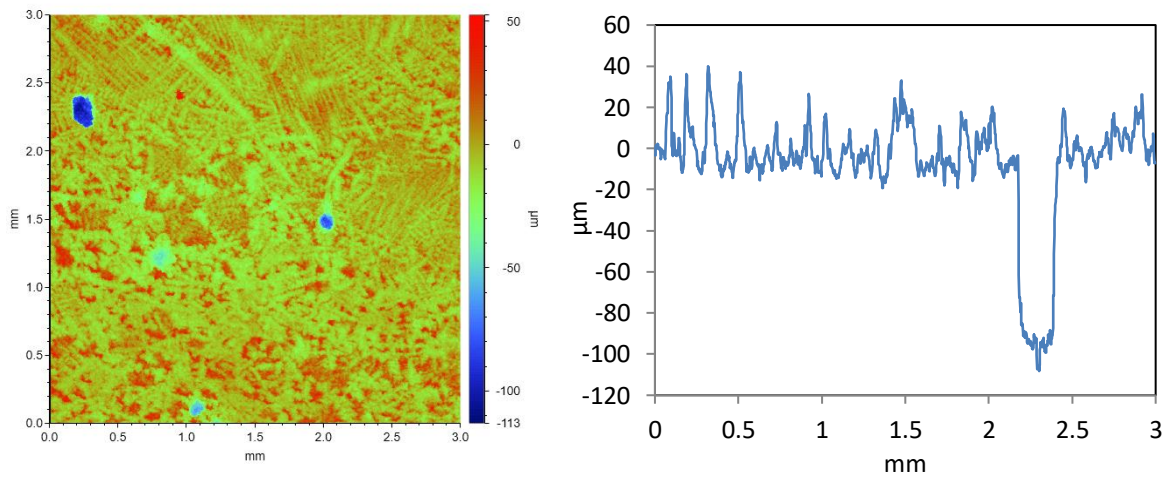
578



579

580

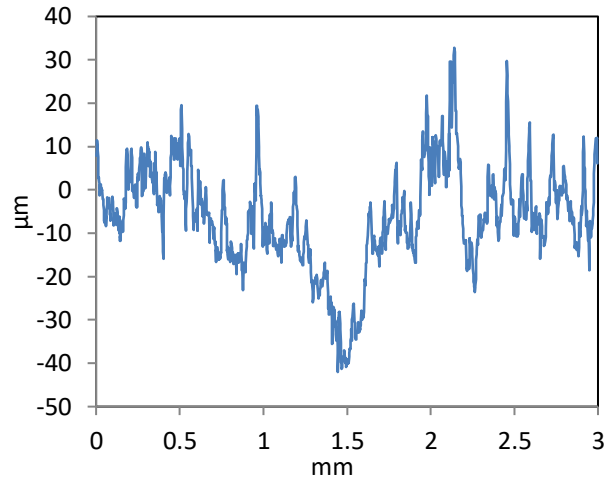
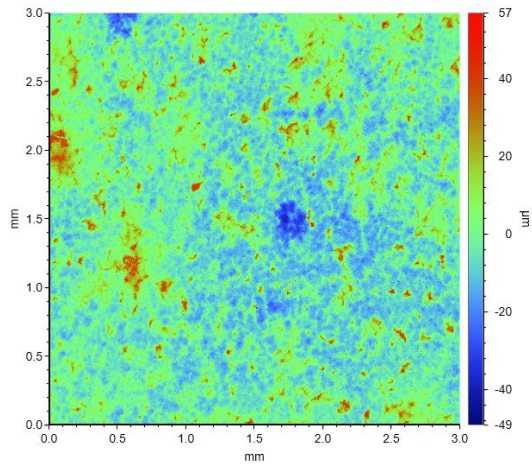
(a)



581

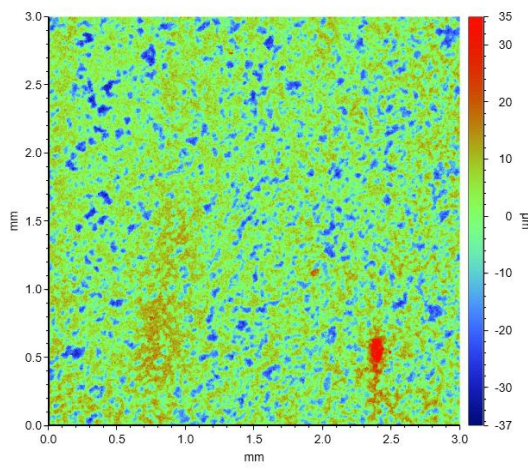
582

(b)

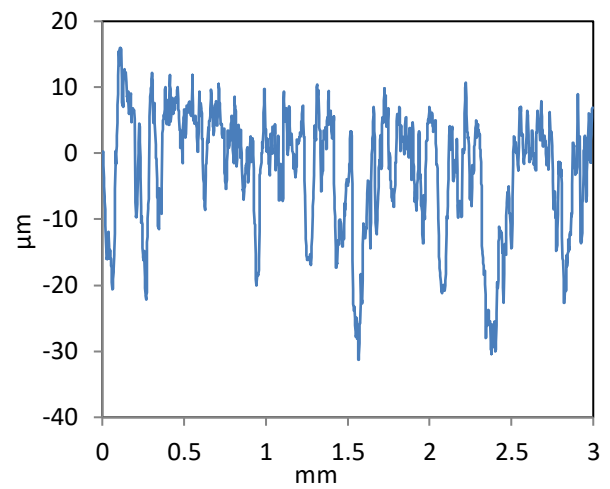


583

584



(c)



585

586

587

588

589

590

591

(d)

**Figure 10: Example of profilometry images for (a) X65, (b) 1Cr, (c) 3Cr and (d) 5Cr steel surfaces after removal of corrosion products after exposure to a CO<sub>2</sub>-saturated 1 wt.% NaCl solution at 100 bar and 60°C for 192 h.**

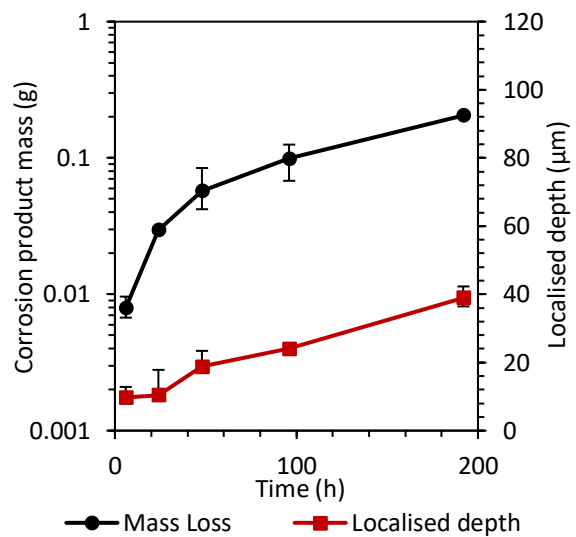
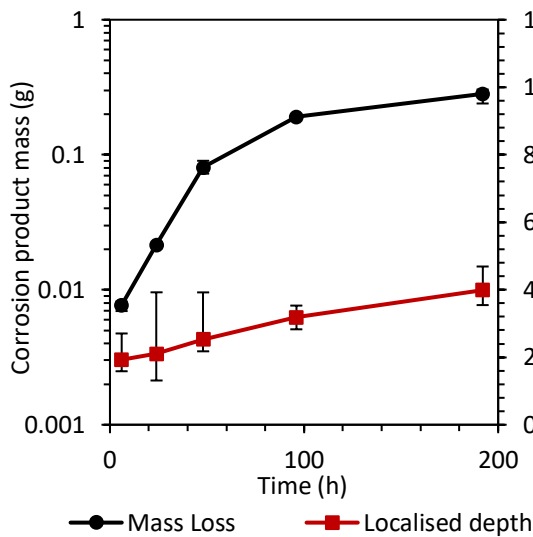
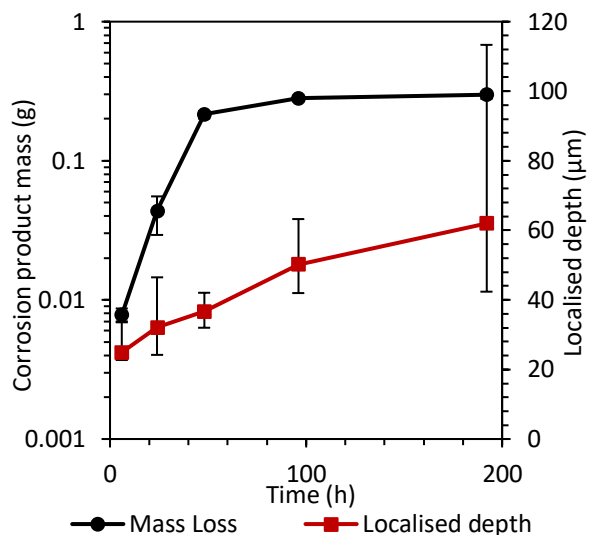
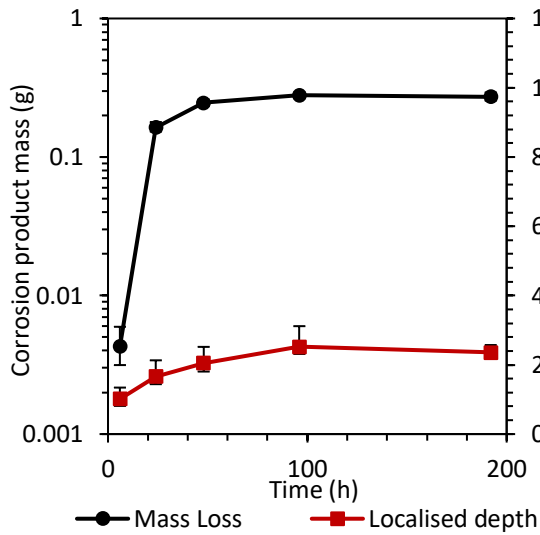
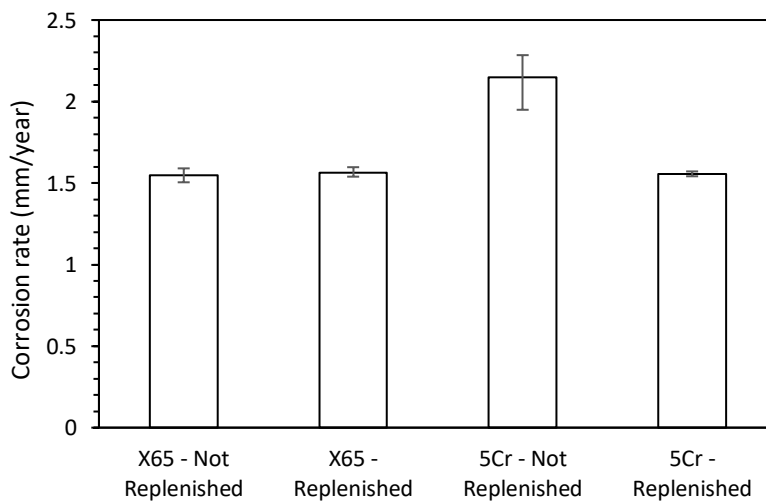


Figure 11: Mass of corrosion products formed on sample surface and measured pit depth for (a) X65, (b) 1Cr, (c) 3Cr and (d) 5Cr exposed to a CO<sub>2</sub>-saturated 1 wt.% NaCl solution at 60 °C and 100 bar at various immersion time.



592  
593

594  
595  
596  
597  
598  
599

600

601 **Figure 12: Corrosion rates for X65 and 5Cr after 192 h exposure to a CO<sub>2</sub>-saturated 1 wt.%**  
602 **NaCl solution at 60 °C and 100 bar. The graphs illustrate the effect of replenishing the test**  
603 **solution after 48 h.**

604

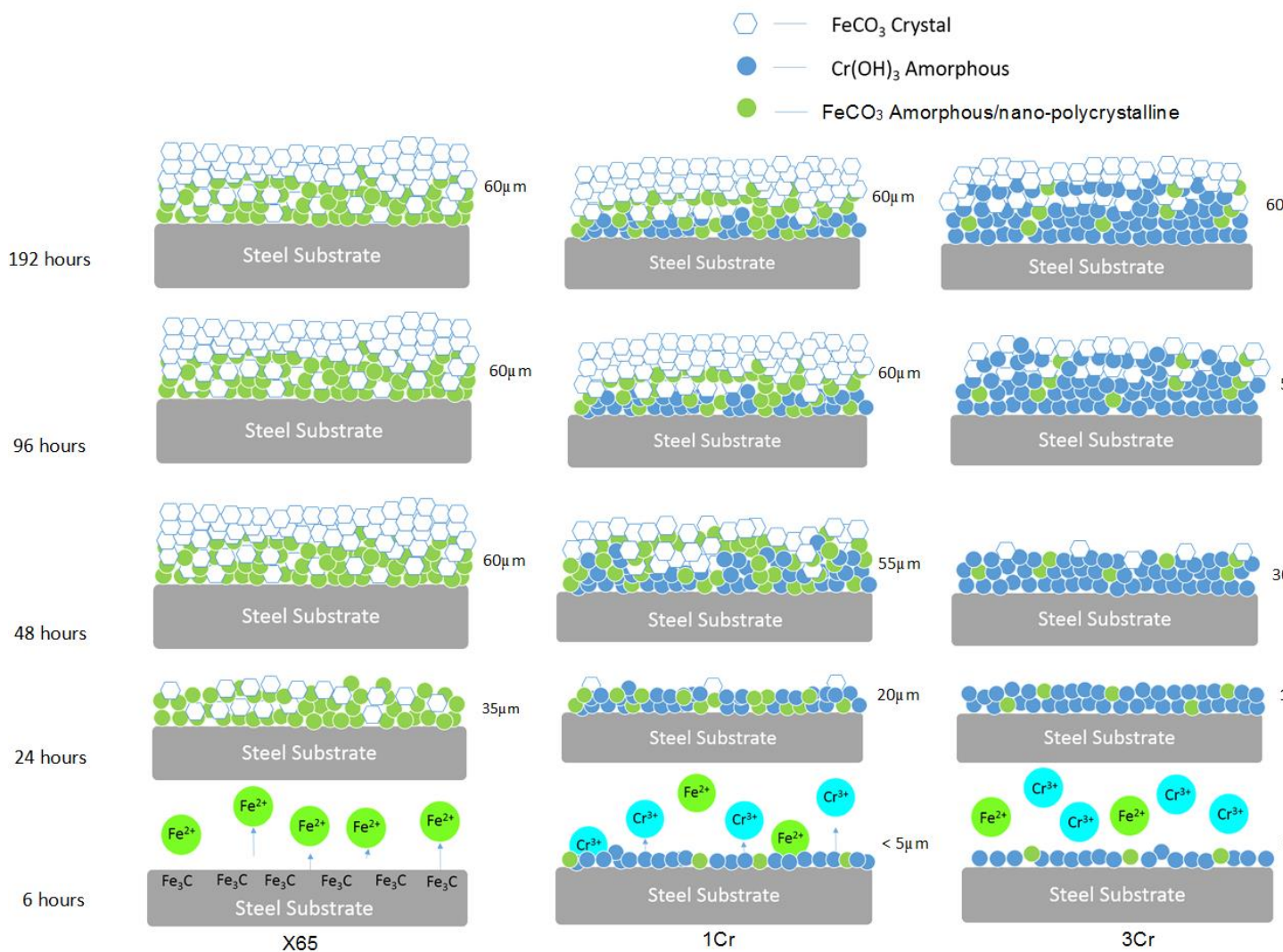


Figure 13: Schematic model for the corrosion product evolution of inner and outer layer on X65, 1Cr, 3Cr and 5Cr steels.



608

609

**Table 1: Elemental compositions of X65, 1Cr, 3Cr and 5Cr steels (wt.%)**

	<b>X65</b>	<b>1Cr</b>	<b>3Cr</b>	<b>5Cr</b>
C	0.12	0.35	0.24	0.35
Si	0.18	0.35	0.21	0.85
Mn	1.27	0.75	0.53	0.4
P	0.008	0.035	0.005	0.012
S	0.002	0.05	0.0015	0.002
Cr	0.11	1.12	3.10	5.00
Fe	Balance			

610

611

612